01 Jan 2007

Neural Network Based Method for Predicting Nonlinear Load Harmonics

Joy Mazumdar

Ronald G. Harley

Frank C. Lambert

Ganesh K. Venayagamoorthy
Missouri University of Science and Technology

Recommended Citation

Neural Network Based Method for Predicting Nonlinear Load Harmonics

Joy Mazumdar, *Member, IEEE*, Ronald G. Harley, *Fellow, IEEE*, Frank C. Lambert, *Senior Member, IEEE*, and Ganesh K. Venayagamoorthy, *Senior Member, IEEE*

Abstract—Generation of harmonics and the existence of waveform pollution in power system networks are important problems facing the power utilities. The increased use of nonlinear devices in industry has resulted in direct increase of harmonic distortion in the industrial power system in recent years. Interaction between loads and sources in a power distribution network is a complex process and often not possible to explain analytically without making assumptions. The determination of true harmonic current distortion of a load is further complicated by the fact that the supply voltage waveform at the point of common coupling (PCC) is rarely a pure sinusoid. This paper proposes a neural network based method to find a way of distinguishing between load contributed harmonics and supply harmonics, without disconnecting any load from the network. A neural network structure with memory is used to model the admittance of the nonlinear load. Once training is achieved, the neural network predicts the true harmonic current of the load if it could be supplied with a clean sine wave. The main advantage of this method is that only waveforms of voltages and currents have to be measured and is applicable for single phase as well as multiphase loads. This could be integrated into a commercially available power quality instrument or be fabricated as a standalone instrument that could be installed in substations of large customer loads, or used as a hand-held clip on instrument.

Index Terms—Neural network, point of common coupling (PCC).

I. INTRODUCTION

THE objective of the electric utility is to deliver a sinusoidal voltage at fairly constant magnitude and frequency throughout its network. However, with the widespread proliferation of power electronic loads, significant amounts of harmonic currents are being injected into the network by these loads. Due to the complex interactions between loads and sources, it is difficult to predict with certainty the origin of the network pollution [1]. The most common approach adopted to tackle this problem was the establishment of limits on the amount of harmonic currents and voltages generated by customers and util-
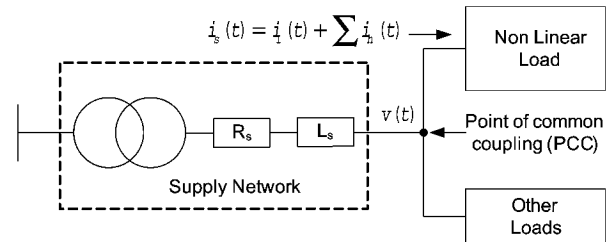
Fig. 1. Typical power distribution network.

ities. The IEEE standard 519 [2], [3] and the IEC-1000-3 [4] are such examples. Customers are required to comply with the regulations and any enforcement by the utility depends on an accurate measurement of the harmonic current injected by the offending customer.

Fig. 1 shows a typical power distribution network. When the nonlinear load is supplied from a sinusoidal voltage source, its injected harmonic current is referred to as contributions from the load. Harmonic currents cause harmonic volt drops in the supply network and therefore distort the voltage at the point of common coupling (PCC). Any loads, even linear loads, connected to the PCC, will have harmonic currents injected into them by the distorted PCC voltage. Such currents are referred to as contributions from the power system, or supply harmonics.

This problem even exists when a single load is connected to the PCC. If the true harmonic current injections from the load were known, then a utility could penalize the offending consumer in some appropriate way, including say a special tariff or insist on corrective action by the consumer. Simply measuring the harmonic currents at each individual load is not sufficiently accurate since these harmonic currents may be caused by not only the nonlinear load, but also by a non-sinusoidal PCC voltage. This is not a new issue and researchers have proposed tools based on traditional power system analysis methods to solve this problem. The harmonic active power method [5] and critical impedance measurement method [6] yield results to a certain degree of accuracy; however they are based on some fundamental assumptions like prior knowledge of the source impedance.

Neural networks have been known to be good function approximators. They are particularly effective in dealing with nonlinear relationships between parameters. This paper presents a different approach [7] based on recurrent neural networks (RNNs) to distinguish between the two components of harmonic sources (i.e., load or power system). Others have in the past proposed methods [8]–[10] to measure the harmonic content in a load current or to predict it, but these methods assume a radial feeder supplying a single load through known

feeder impedance, or multiple loads connected to a PCC which has a sinusoidal voltage and with zero impedance in the supply feeder. The rationale behind using neural networks is that neural networks provide the flexibility of identifying dynamic systems online without the need to make assumptions.

II. RECURRENT NEURAL NETWORK

Artificial neural networks (ANNs) provide an alternative modeling approach for power system applications [11]–[14]. The multilayer perceptron network (MLPN) is one of the most popular topologies in use today [15]. This network consists of a set of input neurons, output neurons and one or more hidden layers of intermediate neurons. Data flows into the network through the input layer, passes through the hidden layers and finally flows out of the network through the output layer. The network thus has a simple interpretation as a form of input-output model, with network weights as free parameters. The use and training of MLPNs is well understood [16].

RNNs are feedback networks in which the present activation state is a function of the previous activation state as well as the present inputs. Adding feedback from the previous activation step introduces a kind of memory to the process. Thus adding recurrent connections to a multilayer perceptron network enhances its ability to learn temporal sequences without fundamentally changing the training process. Recurrent networks will, in general, perform better than regular MLP feedforward networks on systems with transients [17].

The block diagram of a RNN interconnected with weight matrices W and V is shown in Fig. 2. The function $g(., W, V)$ represents the RNN approximation of the plant function $f(\cdot)$ in terms of it weights W and V. The objective of the training is to modify W and V such that the RNN function $g(., W, V)$ approximates the desired function $f(\cdot)$, so that the error e_0 between the desired function output $\hat{y}$ and the RNN output y is minimized.

Continual online training (COT) is required whenever $f(\cdot)$ is a time varying signal and $g(., W, V)$ has to track $f(\cdot)$. The online training cycle has two distinct paths: forward propagation and error back-propagation. Forward propagation is the passing of inputs through the neural network structure to its output. Error back-propagation is the passing of the output error backwards through the RNN in order to estimate the individual contribution of each weight in the network to the final output error. The weights are then modified so as to reduce the output error. The process is repeated at every sampling step. The generalized equations with respect to Fig. 2 are shown as follows.

A. Forward Propagation

At any sampling step k, each input in the input column vector $\underline{x}$ is fed via the corresponding weight in the input weight matrix W to every node in the hidden layer. The activation vector $\underline{a}$ is determined as the sum of its weighted inputs. In vector notation, this is defined as

$$\underline{a} = W\underline{x} \qquad (1)$$

where the input column vector $\underline{x} \in R^{n+m}$, hidden layer activation column vector $\underline{a} \in R^m$, input weight matrix $W \in R^{m \times (n+m)}$, n is the number of inputs to the RNN including the bias and m is the number of neurons in the hidden-layer.
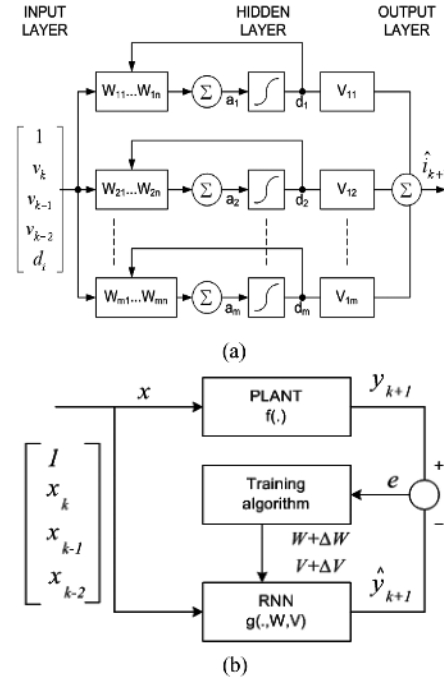

Fig. 2.   (a) RNN architecture and (b) RNN training scheme.

Each of the hidden node activations in $\underline{a}$ is then passed through a sigmoidal function to determine the hidden-layer decision vector $\underline{d}$. A sigmoidal function is defined as

$$sig(\cdot) = \frac{1}{1 + e^{(\cdot)}}. \qquad (2)$$

The hidden-layer decision vector $\underline{d}$ is expressed as

$$d_i = \frac{1}{1 + e^{(-a_i)}}, \quad i \in \{1, 2, \ldots, m\} \qquad (3)$$

where $\underline{d} \in R^m$.

The decision vector $\underline{d}$ is then fed back to the input layer (this introduces the recurrence) as well as fed to the corresponding weight in the output weight matrix W. The RNN output $\hat{y}$ is computed as

$$\hat{y} = (V\underline{d})^T. \qquad (4)$$

For a single output system the output weight matrix $V \in R^{1 \times m}$, and $\hat{y}$ is a scalar.

B. Error Back-Propagation

The output error e_0 is calculated as

$$e_0 = y - \hat{y}. \qquad (5)$$

For a three phase system, $e_0 \in R^{1 \times 3}$.

The output error is back propagated through the RNN to determine the errors $\underline{e}_d$ and $\underline{e}_a$ in the decision vector $\underline{d}$ and activation vector $\underline{a}$. The decision error vector $\underline{e}_d$ is obtained by back-propagating the output error e through the output weight vector V

$$\underline{e}_d = V^T e \qquad (6)$$

where the decision error vector $\underline{e}_d \in R^m$.

TABLE IRNN EXECUTION CYCLE COMPUTATIONS

Equation	Multiplication	Addition	Sigmoidal
(1)	m(m+n)	m(m+n)	0
(2)	0	0	m
(3)	m	m	0
Forward Propagation	m(m+n+1)	m(m+n+1)	m
(4)	0	1	0
(5)	m	m	0
(6)	2m	0	0
(7): ΔV	2m+1	m	0
(7): ΔW	m(2m+2n+1)	m(2m+2n+1)	0
(8)	0	m(m+n)+m	0
Error Backpropagation	~m(2m+2n+5)	~2m(m+n+1)	0

The activation errors e_{ai} are given as a product of the decision errors e_{di} and the derivative of the decisions d_i with respect to the activations a_i

$$
\begin{aligned}
e_{ai} &= \left(\frac{d}{da_i} d_i \right) e_{di} \\
&= \left(\frac{d}{da_i} \left(\frac{a}{1+e^{(-a_i)}} \right) \right) e_{di} \\
&= d_i(1-d_i)e_{di}, \quad i \in \{1,2,\ldots,m\}.
\end{aligned} \tag{7}
$$

The derivative of a sigmoidal function can be expressed in terms of its inputs and outputs and computationally it results in multiplication and addition. The subscript i in (7) indicates element-wise multiplication of the vectors $\underline{d}$, $\underline{1-d}$ and $\underline{e}_d$.

The change in input weights ΔW and output weights ΔV at step k are calculated as

$$
\begin{aligned}
\Delta W(k) &= \gamma_m \Delta W(k-1) + \gamma_g \underline{e}_a \underline{x}^T \\
\Delta V(k) &= \gamma_m \Delta V + \gamma_g \underline{e}_y \underline{d}^T
\end{aligned} \tag{8}
$$

where $\gamma_m, \gamma_g \in [0,1]$ are the momentum and learning gain constants respectively. The last step in the training process is the actual updating of the weights at step k

$$
V(k) = V(k-1) + \Delta W(k). \tag{9}
$$

C. Execution Cycle Computation

All the necessary (1)–(8) are computed in vector form. Most of the computations involve either addition or multiplication. Evaluation of the sigmoidal function is the only computationally demanding task. A complete breakdown of the computations required for one RNN execution cycle appears in Table I which shows that the forward propagation requires m sigmoidal computations.

D. Optimum Sizing of the RNN

To model the harmonic characteristics of a nonlinear load, the RNN architecture needs to address the issues regarding, 1) the number of layers, 2) number of neurons in each layer, and 3) the hidden layer activation function. For any nonlinear function identification type problem, at least one hidden layer is required. Additionally, a nonlinear, continuously differentiable hidden layer activation function, such as the sigmoidal function, allows the network to perform nonlinear modeling. Depending on the application, the number of RNN inputs and the number

of outputs are fixed. The only structural variable then remaining is the number of neurons m in the hidden layer. The RNN execution time and the training convergence is directly dependent on the value of m. Two performance criteria for the measure of RNN training convergence are typically used; they are the absolute value of the tracking error T_e defined as

$$
T_e = |(y - \hat{y})| \tag{10}
$$

and the mean squared error (MSE) defined as

$$
\text{MSE} = \frac{1}{r} \sum_1^r |(y - \hat{y})|^2 \tag{11}
$$

where r is the number of training epochs. The tracking error T_e varies at a high rate as training progresses. For this reason it is more convenient to consider the MSE which is a smooth curve due to the averaging process. In neural network training it is not possible to get MSE to decrease to exactly zero, so the objective is to get it down below some minimum value, typically ($\text{MSE}_{\min} < 10^{-2}$). This can be achieved by providing information to the neural network about the history of the system dynamics, typically in the form of delayed inputs and outputs.

The number of neurons in the hidden layer affects the rate and the final value of the MSE convergence, and is typically chosen on a heuristic basis after several iterations. For the specific problem presented in this paper, based on experimental data and experience, the following formula provides a starting point for choosing the number of neurons in the hidden layer

$$
H_n \leq \frac{C \cdot \text{MSE}_{\min}}{S} \tag{12}
$$

where H_n is the number of neurons in the hidden layer, C is the number of cycles of training data, $\text{MSE}_{\min}$ acceptable MSE in training expressed in % and S is the number of samples per cycle of the acquired data. The above formula has been adapted from work of Baum and Haussler [18] and its application is demonstrated below.

Typically power quality recording instruments like the AVO Megger PA-9Plus, the RPM and others, require data to be sampled at 128 samples/ cycle. Starting with random initial values for the RNN weights, and to achieve a $\text{MSE}_{\min}$ of 0.5% with only 120 cycles of acquired data at 128 samples/cycle, the number of neurons in the hidden layer works out to be ≤ 28. For the work presented in this paper, the number of neurons used in the hidden layer is 25.

III. ESTIMATION OF HARMONIC CURRENT

Fig. 3 is a one-line diagram of a three-phase supply network with a sinusoidal voltage source v_s, network impedance L_s, R_s and several loads (one of which is nonlinear) connected to a PCC. The nonlinear load currents i_a, i_b, and i_c, (denoted by i_{abc}), are composed of load harmonics as well as supply harmonics. However the utility sees the line current i_{abc} as the harmonic distortion injected into the network by the load. The identification recurrent neural network (RNN1) is trained to identify the nonlinear characteristics of the load (in the case of a single phase load), and for each phase individually for a three-phase load. At any moment in time after the RNN1 training has been completed, its weights are transferred to the estimation recurrent neural network (RNN2). RNN2 is then supplied offline with
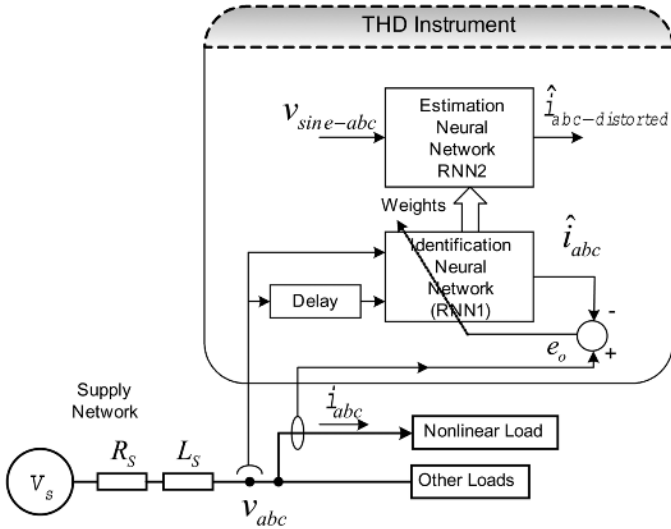
Fig. 3. Proposed method for predicting the true harmonic distortion of a nonlinear load.

a three-phase mathematically generated sine wave $v_{\sin e-abc}$ to estimate its three output currents $\hat{i}_{abc-\mathrm{distorted}}$. Any distortion present in the current waveforms $\hat{i}_{abc-\mathrm{distorted}}$ can now truly be attributed to the nonlinearity of the load admittance. This procedure is known as load modeling. The function of RNN2 could have been carried out by RNN1, but that would disrupt the continual online training of RNN1 during the brief moments when $\hat{i}_{abc-\mathrm{distorted}}$ has to be estimated. The algorithms of RNN1 and RNN2 are executed in software.

A. Identification Phase: RNN1 Training

The proposed method measures the instantaneous values of the three voltages v_{abc} at the PCC, as well as the three line currents i_{abc} at the kth moment in time. The voltages v_{abc} could be line-to-line or line-to-neutral measurements. The RNN1 is designed to predict one step ahead the line current $\hat{i}_{abc}$ as a function of the present and delayed voltage vector values $v_{abc}(k)$, $v_{abc}(k-1)$ and $v_{abc}(k-2)$. When the $k+1$ moment arrives (at the next sampling instant), the actual measured instantaneous values of i_{abc} are compared with the previously predicted values of $\hat{i}_{abc}$, and the difference (or error e) is used to train the RNN1 weights. This is called continual online training.

Initially the weights have random values, but after several sampling steps, the training soon converges and the value of the error e in Fig. 3 diminishes to an acceptably small value, as expressed by the value of MSE. Proof of this is illustrated by the fact that the individual phase waveforms for i_{abc} and $\hat{i}_{abc}$ should practically lie on top of each other respectively. At this point the RNN1 therefore represents the admittance of the nonlinear load. This process is called identifying the load admittance. Since continual online training is used, it will correctly represent the load admittance from moment to moment. At any moment in time after the RNN1 training has converged, its weights are transferred to RNN2. The training cycle of RNN1 continues and in this way RNN2 always has updated weights available when needed.

B. Estimation Phase: RNN2 Prediction

RNN2 is supplied with a mathematically generated sine wave to estimate its output while its weights are kept fixed. The output of RNN2 called $\hat{i}_{abc-\mathrm{distorted}}$ therefore represents the current which the nonlinear load would have injected had it been supplied by a sinusoidal voltage source at the PCC. In other words, this gives the same information that could have been obtained by quickly removing the distorted PCC voltage (if this were possible) and connecting a pure sinusoidal voltage to supply the nonlinear load, except that it is not necessary to actually do this interruption. Any distortion present in the $\hat{i}_{abc-\mathrm{distorted}}$ waveform can now be attributed to the nonlinearity of the load admittance. Once a number of $\hat{i}_{abc-\mathrm{distorted}}$ cycles have been calculated by RNN2, they are stored (and subsequently used for harmonic analysis to find the true load-injected current total harmonic distortion $(\mathrm{THD})_i$). New weights are then uploaded from RNN1 to RNN2, and a series of new $\hat{i}$ cycles and a new THD_i calculated. The THD_i value could be recorded or displayed at frequent pre-determined intervals, or an average value calculated over a period of time, say every 5 min or as required.

C. Scaling the RNN Variables

Due to the nature of the sigmoidal transfer function, the outputs of the neurons in the hidden layer are limited to values between 0 and 1. The inputs to the neural networks are therefore scaled first to fall within the limits of ± 1. Scaling is done using software and therefore removes any restrictions placed on the data acquisition system and the transducers.

IV. EXPERIMENTAL RESULTS

The method of using online trained RNNs to identify the load admittance, and testing it, is briefly introduced. Nonlinear loads are typically caused by switching power devices at the interface between the supply network and the load, or by motor or transformer saturation. The performance of the RNN is demonstrated with the help of the simple nonlinear load test system in Fig. 4.

The proposed scheme is demonstrated with three single phase loads connected to a switch S defined as the point of common coupling. The voltage at the PCC is fixed at 120 Vrms, 60 Hz. When S is in position 1, the power supply comes from the utility supply network. When S is in position 2, the supply comes from a 5 kVA California Instruments 5001 iX power supply which provides a "clean" sinusoidal voltage at the PCC. The background THD of the utility voltage is 4.19% (with S open) and the THD of the CI 5001 iX voltage is 0.2%.

Table II shows the individual harmonic generation characteristic (THD) of each load in Fig. 4 when connected one at a time first to the clean supply and then to the distorted voltage from the utility.

THD is measured by a dedicated spectrum analyzer as well as by data acquisition and MATLAB software. Data acquisition is carried out with a system from National Instruments and LABVIEW software which stores the data on a personal computer. This data is then imported to MATLAB and, using the *powergui* block of SIMULINK, the THD's are computed. These THDs are then compared with measurements taken directly by the spectrum analyzer, in order to verify that the LABVIEW and MATLAB computer code are working correctly.
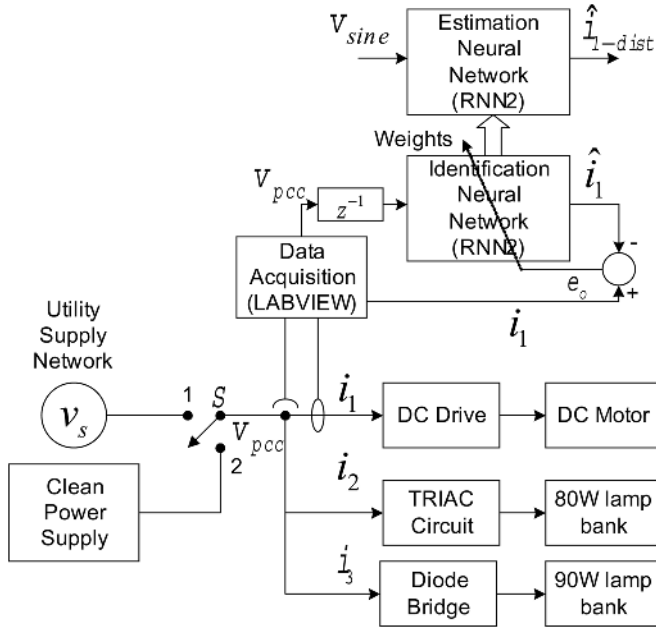
Fig. 4. Experimental setup with two nonlinear loads and one linear load.

TABLE II
SAMPLE MEASUREMENT DATA USING 5001
IX TO SUPPLY ONE LOAD AT A TIME

Load Type	Clean Supply		Distorted Supply	
	v_{pcc}	i_{load}	v_{pcc}	i_{load}
TRIAC with 0° firing angle (i_1)	0.2%	4.28%	4.19%	6.11%
TRIAC with 30° firing angle (i_1)	0.2%	30.42%	4.19%	29.25%
80W Lamp (i_2)	0.2%	0.34%	4.19%	4.25%
Diode rectifier with 90 W lamp (i_3)	0.2%	0.39%	4.19%	4.32%

An important result from Table II is that the current THD of the dimmer circuit with 30° firing angle is higher when it is being supplied by the clean supply (less THD in v_{pcc}) as compared to when it is supplied by the utility (more THD in v_{pcc}). However with 0° firing angle, the result is the other way round. Ideally, linear loads do not introduce harmonics in the network but do get affected by the distortion in the supply voltage.

When several loads are supplied from the PCC, with its own background THD, the individual load currents are due to the combined effects of the distorted and the nonlinearities of the loads. This results in some amount of phase cancellation between supply harmonics and load harmonics, or load harmonics from one load cancelling those of another load. This cancellation reduces the overall harmonic current in the network [19] and thus benefits some of the nonlinear loads. Hence, it is essential that any method of measuring load harmonic contribution should be able to analyze every load on its merit.

A. TRIAC Dimmer Circuit

With the firing angle of the dimmer circuit set to 0° and switch S in position 1 and all the loads in Fig. 4 operating, RNN1 is trained to learn the characteristics of the dimmer circuit. The input to RNN1 is v_{pcc} and the output of RNN1, $\hat{i}_i$, tracks the actual current i_1 until the training error converges to near zero.
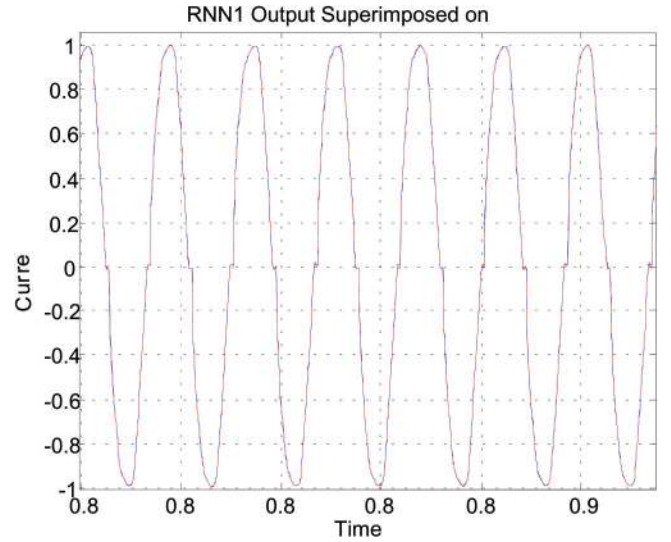

Fig. 5. RNN1 training result with 0° firing angle; i_1 and $\hat{i}_1$ superimposed.
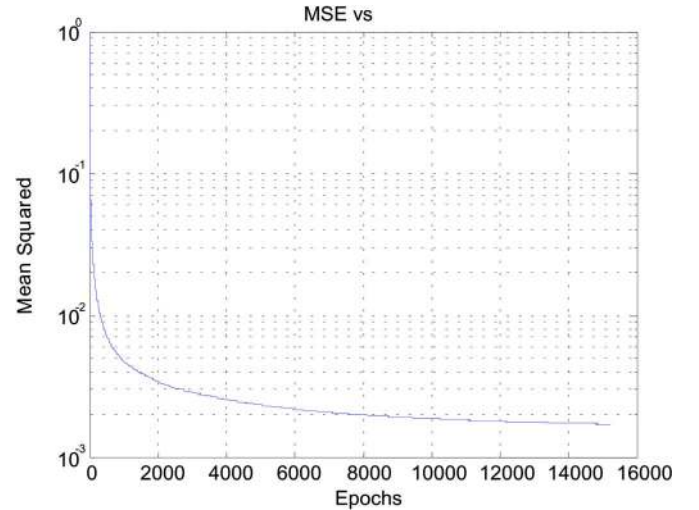

Fig. 6. MSE in RNN1 training of current i_1.

Fig. 5 indicates how well the RNN1 training has converged since its output $\hat{i}_1$ coincides with the actual i_i waveform.

The MSE in Fig. 6 is 0.0021. Once the MSE is below the pre-defined level $\text{MSE}_{\min}(< 10^{-2})$, it can be concluded that RNN1 has learned the admittance of the dimmer circuit to an acceptable degree of accuracy. The weights of RNN1 are now transferred to RNN2. RNN2 is now supplied with a mathematically generated sine wave voltage with zero distortion. The output of RNN2 is $\hat{i}_{1-\text{dist}}$ and it appears in Fig. 7 which shows what Fig. 5 would have looked like if it were possible to isolate the dimmer circuit and supply it by a pure sine wave. In other words this is the true harmonic current that would be injected by the dimmer circuit into the network if the PCC voltage had no distortion.

The true current THD of $\hat{i}_{1-\text{dist}}$ in Fig. 8 turns out to be 4.18% instead of 6.11% measured in Fig. 5. This result agrees well with the measured value of 4.28% obtained where the load was supplied by a 0.2% distorted voltage when switch S was in position 2 in Fig. 4 and only the dimmer circuit was connected to S.
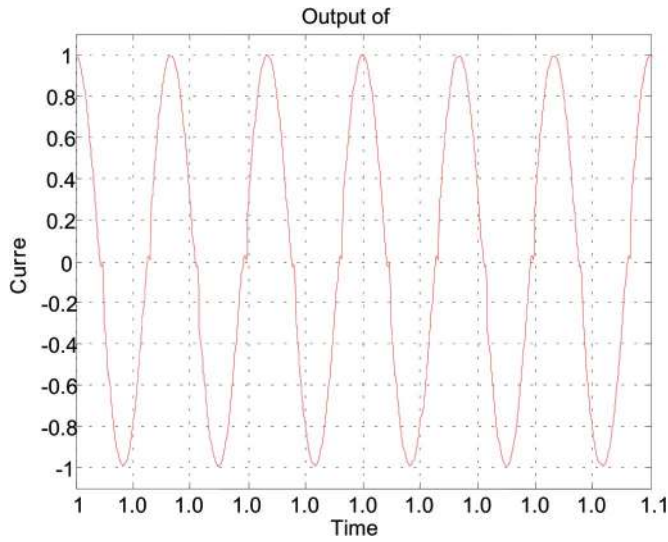
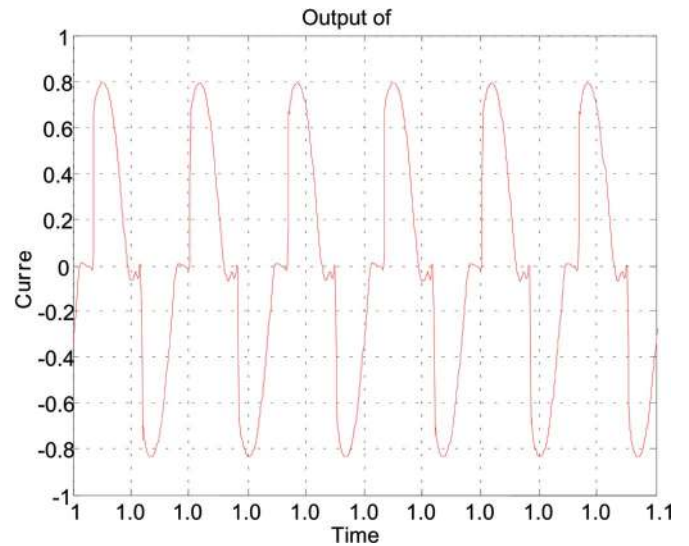Fig. 7.   RNN2 output $\hat{i}_{i-\text{dist}}$ when supplied by pure sine wave.
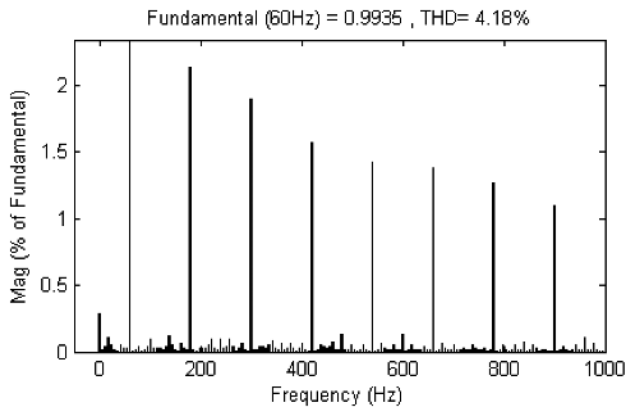
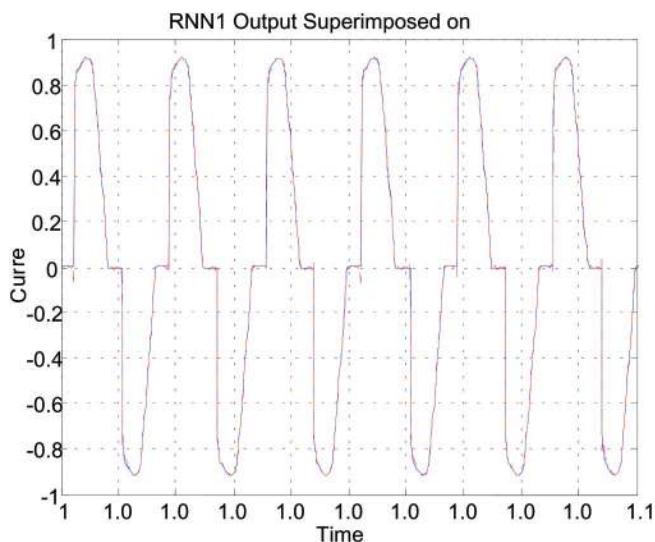Fig. 8.   FFT spectrum of $\hat{i}_{1-\text{dist}}$ (THD $= 4.18\%$).
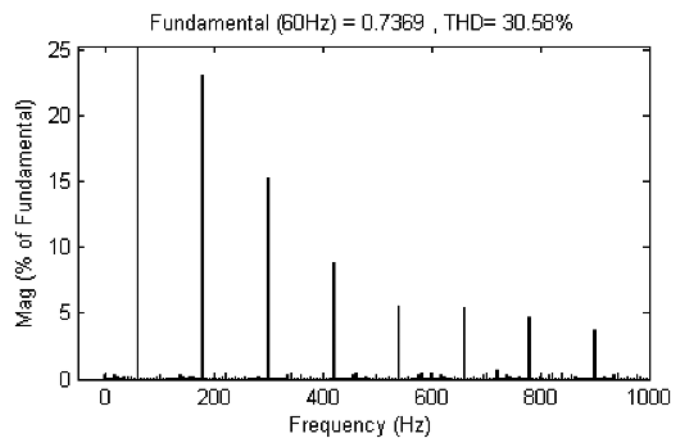
Fig. 9.   RNN1 training result with $30°$ firing angle; i_1 and $\hat{i}_1$ superimposed.

Similarly, the data obtained by operating the dimmer circuit with a $30°$ firing angle is used to train RNN1 and the convergence result is shown in Fig. 9. The weights of RNN1 are trans-

Fig. 10.   RNN2 output $\hat{i}_{1-\text{dist}}$ when supplied by pure sine wave.

Fig. 11.   FFT spectrum of $\hat{i}_{1-\text{dist}}$ (THD $= 30.58\%$).

ferred to RNN2 and again it is supplied with a pure mathematically generated sine wave voltage. The output of RNN2 is shown in Fig. 10 and its FFT in Fig. 11. The true current THD of $\hat{i}_{1-\text{dist}}$ in Fig. 11 turns out to be 30.58% instead of 29.25% as measured in Fig. 9. This result agrees well with the measured value of 30.42% obtained where the load was supplied by a 0.2% distorted voltage with S in position 2 and only supplying the dimmer circuit.

B. Variable Speed Drive

The proposed scheme is now applied to a three phase variable speed drive (VSD) system feeding an induction motor as shown in Fig. 12. The background THD of the utility voltage with S open is 4.5%, and the background THD of the CI 5001 iX voltage is 0.2%.

With switch S in position 1, the VSD is supplied from the utility source, and with S in position 2, the drive is supplied from the clean power source. The measured phase A voltage and current waveforms with S in position 1 are shown in Fig. 13, while Fig. 14 contains the measured phase A voltage and current waveforms with S in position 2. The THD of the current with S in position 1 is 74.27% and THD of the current with S in
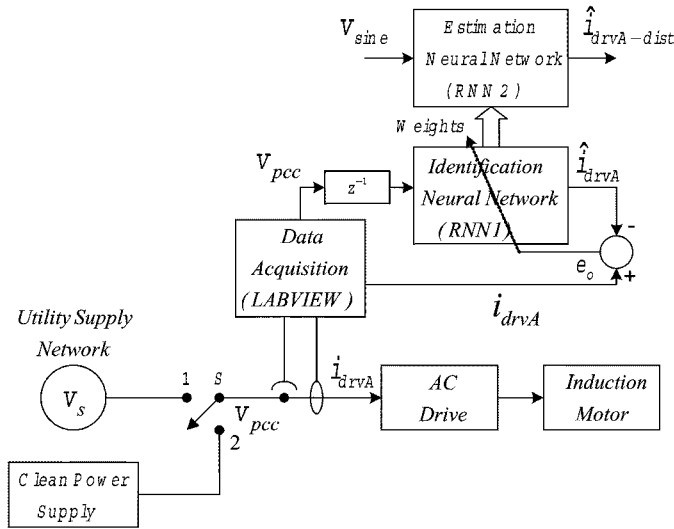
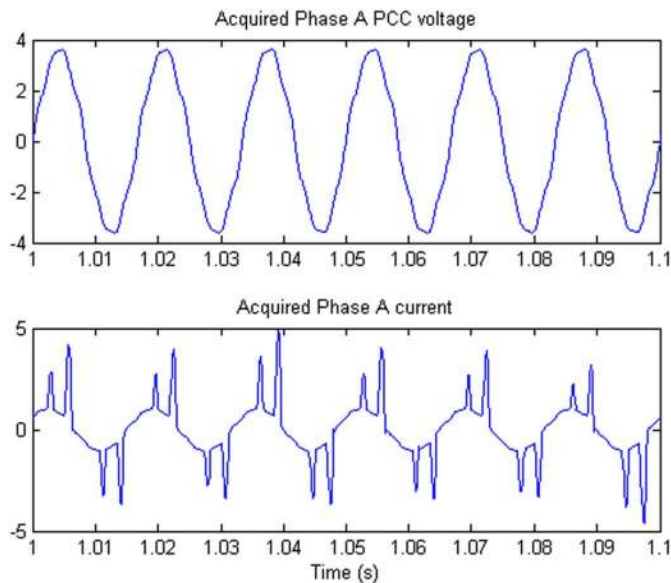Fig. 12.   Experimental setup with a variable speed drive.

Fig. 14.   Measured voltage and current with S in position 1.

Fig. 13.   Measured voltage and current with S in position 1.

Fig. 15.   FFT Spectrum of current i_{drvA} with S in position 1 (THD = 74.27%).
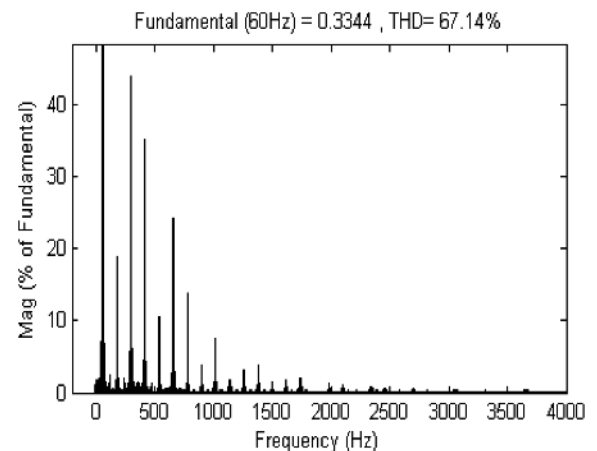
Fig. 16.   FFT Spectrum of current i_{drvA} with S in position 1 (THD= 67.14%).

position 2 is 67.14%. The FFT spectrums are shown in Figs. 15 and 16, respectively.

The data obtained with S in position 1 is used to train the neural network RNN1 until the training error converges to near zero, and the output of RNN1 correctly tracks the actual current i_{drvA}. Fig. 17 indicates how well the training of RNN1 has converged since its output $\hat{i}_{drvA}$ coincides with the actual i_{drvA} waveform. Fig. 18 shows how the MSE in RNN1 decreases as the training converges.

Once training is complete, and RNN1 has learned the admittance of the phase A of the VSD, the weights of RNN1 are transferred to RNN2. As before, the output of RNN2 $\hat{i}_{drvA-dist}$ is obtained by using a mathematically generated sine wave voltage with zero distortion as its input and Fig. 19 shows what Fig. 17 would have looked like if it were possible to isolate the VSD and supply it from a pure sine wave voltage.

Fig. 20 contains the frequency spectrum of Fig. 19. The true current distortion of $\hat{i}_{1-dist}$ turns out to be 66.69% (instead of
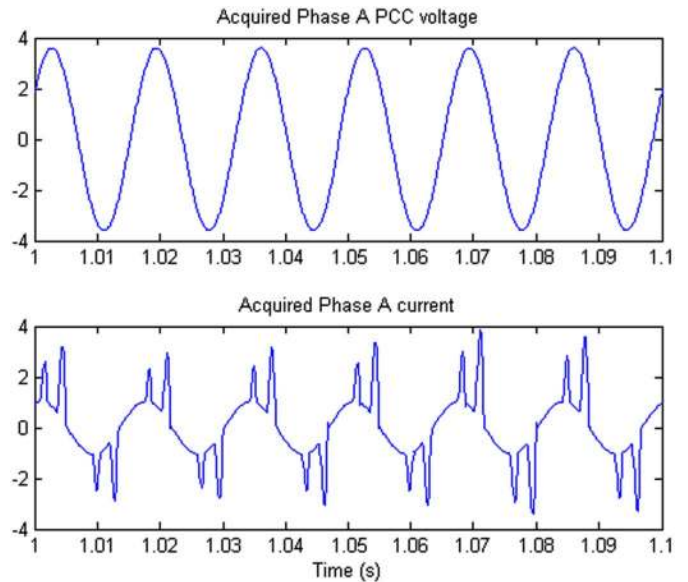
the 74.27% of Fig. 17). This result agrees well with the measured value of 67.14% of Fig. 14 where the VSD was supplied by a 0.2% distorted voltage.

Fig. 17. RNN1 training result of VSD; i_{drvA} and $\hat{i}_{drvA}$ superimposed.

Fig. 18. MSE in RNN1 training with VSD.

Fig. 19. RNN2 output $\hat{i}_{drvA-\text{dist}}$ when supplied by pure sine wave.

The results above of the three different load types, have shown that there is a difference in the current distortion of a load depending on whether the load is served by a clean supply or a distorted supply. Any load serviced by a utility is designed and optimized to operate at 60 Hz, however once it is connected to the

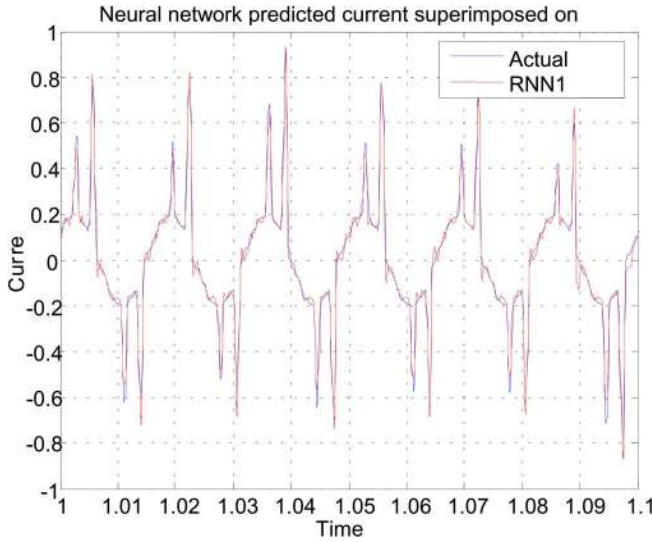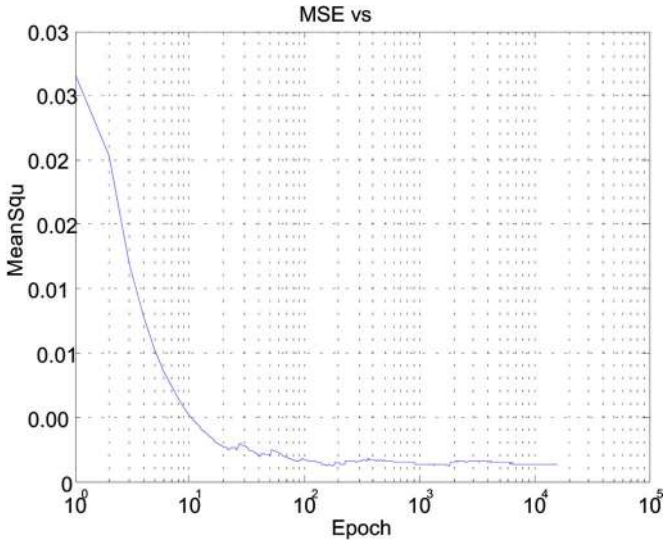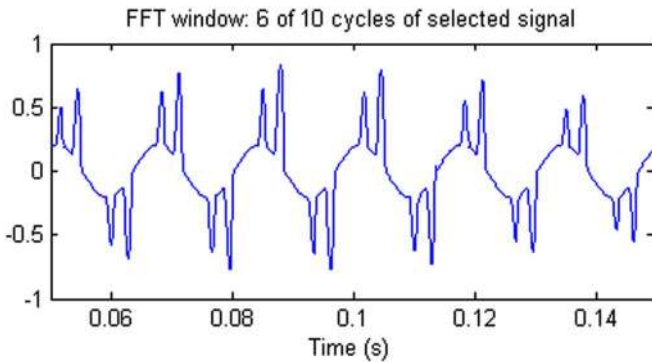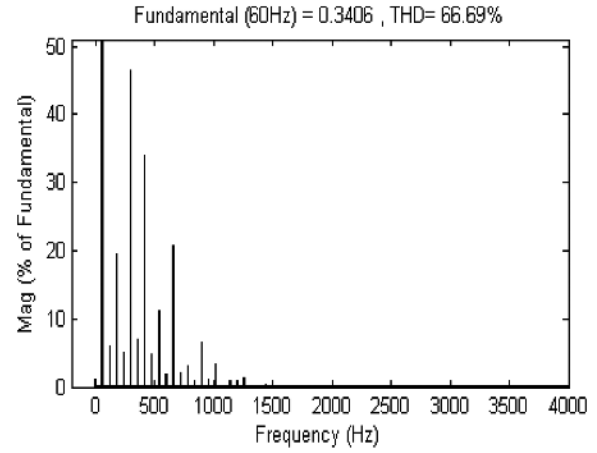Fig. 20. Frequency spectrum of Fig. 19

TABLE III
SUMMARY OF RESULTS

Load	THD_d	THD_s	THD_{C1}	$e_m = \left(\frac{THD_s - THD_d}{THD_s} \right)$
TRIAC with 0° firing angle	6.11%	4.18%	4.28%	-46.17%
TRIAC with 30° firing angle	29.25%	30.58%	30.42%	4.35%
Phase A of VSD	74.27%	66.69%	67.14%	-11.37%

power system network, it rarely receives a clean 60 Hz supply. For the purpose of quantification of this difference, a new parameter e_m, known as the resultant error in measurement, is introduced and defined as

$$e_m = \left(\frac{\text{THD}_s - \text{THD}_d}{\text{THD}_s} \right) \% \qquad (13)$$

where THD_d is i_{THD} from a distorted v_{pcc}, and THD_s is i_{THD} from a mathematical sine wave.

The salient results of the three experiments above are summarized in Table III. THD_{c1} is the distortion in current with the switch S in position 2. This value is used for validation of the results obtained using the proposed scheme. In an actual implementation of the proposed scheme, the value of will not be required since it is not used in the training algorithm nor will such a sine wave source be available in any real power system application.

The values of e_m illustrate that this error could be positive as well as negative. Single-phase power electronic loads generate a great amount of triplen harmonics, and triplen harmonics are zero sequence. Three phase power-electronic loads on the other hand, do not generate triplen harmonics. Non-triplen harmonics generated by various single and three-phase loads are likely to have diversity effects due to phase cancellations and attenuation effects that cause the distortion variation in the PCC voltage. This explains why the index of (13) is either positive or negative. One important finding from the above results show that it is erroneous to reason intuitively that the current THD, when supplied from a distorted v_{pcc} should always be higher than if the v_{pcc} had no distortion.

The significant current harmonics in power electronics loads are almost always fifth, seventh, 11th, or 13th. For applications like dominant harmonic active filtering [20], it may be of interest

TABLE IV
MODELING OF INDIVIDUAL HARMONICS

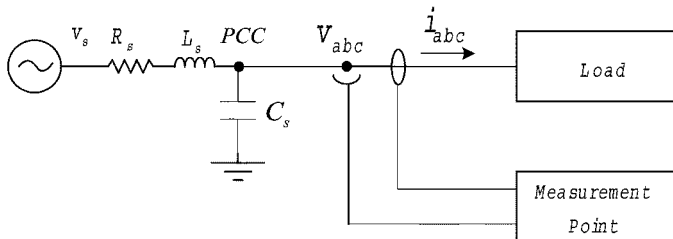| Phase A of VSD	THD_d (% of Fundamental)	THD_s (% of Fundamental)	$e_m = \left(\dfrac{THD_s - THD_d}{THD_s} \right)$
5th Harmonic	41.98%	43.69%	3.91%
7th Harmonic	38.22%	35.00%	-9.20%
11th Harmonic	29.44%	24.35%	-20.90%
13th Harmonic	20.02%	13.86%	-44.44%

Fig. 21.　Three phase power distribution network

to use individual harmonic current distortion in e_m instead of the overall harmonic current distortion. Table IV shows the value of e_m for each dominant harmonic, computed from the experiment result of the variable speed drive current i_{drvA}.

Fig. 21 shows a single line diagram of a typical three phase power distribution network and the point of measurement for the application of the proposed scheme. The scheme uses the values of voltage and current at the point of metering for each customer. It is therefore applicable to both current and voltage source type harmonic loads [21]. The load could consist of numerous non-linear loads including gate controlled drives inside a large plant. However, due to harmonic cancellations as explained above, the net distortion in i_{abc} is always lower and fairly constant compared to that of the individual drives [22]. The scheme in its present form is applicable and valid for loads with fairly constant harmonic spectrum. An example of a time varying load would be an arc furnace and the scheme has not yet been applied on such a load.

The sampling frequency for data acquisition is 8 kHz which ensures that harmonics up to 4 kHz can be measured with sufficient accuracy. Harmonics above that are normally filtered out by filters. The voltage transducers used are LEM LV 25-P and the current transducers used are LEM LAH 25-NP. Some of the experimental details of the RNN implementation are given as follows.

- Recurrent neural network implemented in MATLAB.
- FFT computation: *powergui* block of SIMULINK.
- Number of Neurons in the hidden layer: 25. During the commercialization phase of this work, selection of number of neurons will be worked out in greater details.
- Computation time for the MATLAB code with 16000 samples of acquired data, run on a 1.8 GHz PC: 4.8 s.

V. CONCLUSION

This paper demonstrated the ability of recurrent neural networks to learn the load admittance and utilize a trained neural network for estimating the true harmonic distortion caused by

that load. The proposed method has been successfully applied to some specific single and three phase loads. The advantages of the proposed method are that it can be implemented online without disrupting the operation of any load, only voltages and currents need to be measured, it does not require any special instruments, and it does not need to make any assumptions about any quantities, e.g., the impedance of the source, or a sinewave PCC voltage. Every customer has individual power meters and hence it is a feasible option to implement the scheme for each customer individually.

Standards like IEEE 519 provide guidelines for regulating harmonic distortion levels that divide the responsibility between the utility and the customer. The utility has to maintain voltage distortion at the PCC below the specified limits and the customer has to limit the amount of harmonic current injection onto the utility system. However, disputes may arise between utilities and customers regarding who is responsible for the harmonic distortions due to the lack of a reliable single index which can precisely point out the source and magnitude of the harmonic pollution.

Experimental results presented in this paper confirm that an error in the measurement is made if the calculation of current THD is done by simply measuring the current of the nonlinear load. The information provided by the proposed method regarding the true current distortion of a load could be used to persuade an offending load to take steps to mitigate an unacceptably high level of distortion. The proposed scheme could be integrated into a commercially available power quality instrument or be fabricated as a standalone instrument that could be installed in substations of large customer loads, or used as a hand-held clip on instrument.

REFERENCES

[1] W. M. Grady, A. Mansoor, E. F. Fuchs, P. Verde, and M. Doyle, "Estimating the net harmonic currents produced by selected distributed single-phase loads: Computers, televisions, and incandescent light dimmers," in *Proc. IEEE Power Eng. Soc. Winter Meeting*, Jan. 2002, vol. 2, pp. 1090–1094.

[2] *IEEE Recommended Practices and Requirements for Harmonic Control in Electric Power Systems*, IEEE Standard 519-1992, 1992.

[3] M. McGranaghan, "Overview of the guide for applying harmonic limits on power systems—IEEE 519A," in *Proc. IEEE Int. Conf. Harmonics Qual. Power*, Oct. 1998, vol. 1, pp. 462–469.

[4] *Electromagnetic Compatibility (EMC)-Part 3: Limits-Section VI:Assessment of Emission Limits for Distorting Loads in MV and HV Power Systems*, IEC 1000-3-6,1996, 1996.

[5] W. Xu, X. Liu, and Y. Liu, "An investigation on the validity of power-direction method for harmonic source determination," *IEEE Trans. Power Delivery*, vol. 18, no. 1, pp. 214–219, Jan. 2003.

[6] Li Chun, W. Xu, and T. Tayjasanant, "A critical impedance based method for identifying harmonic sources," *IEEE Trans. Power Delivery*, vol. 19, no. 2, pp. 671–678, Apr. 2004.

[7] J. Mazumdar, R. Harley, F. Lambert, and G. K. Venayagamoorthy, "Using a neural network to distinguish between the contributions to harmonic pollution of non-linear loads and the rest of the power system," in *Proc. IEEE Power Electron. Spec. Conf. (PESC'05)*, Recife, Brazil, Jun. 2005, pp. 366–371.

[8] T. A. George and D. Bones, "Harmonic power flow determination using the fast fourier transform," *IEEE Trans. Power Delivery*, vol. 6, no. 2, pp. 530–535, Apr. 1991.

[9] Y. Baghzouz and O. T. Tan, "Probabilistic modeling of power system harmonics," *IEEE Trans. Ind. Appl.*, vol. IA-23, no. 1, pp. 173–180, Jan./Feb. 1987.

[10] H. Mori and S. Suga, "Power system harmonics prediction with an artificial neural network," in *Proc. IEEE Int. Symp. Circuits Syst.*, Jun. 1991, vol. 2, pp. 1129–1132.

[11] M. Rukonuzzaman, A. A. M. Zin, H. Shaibon, and K. L. Lo, "An application of neural network in power system harmonic detection," in *Proc. IEEE Int. Joint Conf. Neural Networks (IJCNN 1998)*, May 1998, vol. 1, pp. 74–78.

[12] S. Osowski, "Neural network for estimation of harmonic components in a power system," *Proc. Inst. Elect. Eng.*, vol. 139, no. 2, pp. 129–135, Mar. 1992.

[13] W. W. L. Keerthipala, L. T. Chong, and T. C. Leong, "Artificial neural network model for analysis of power system harmonics," in *Proc. IEEE Int. Conf. Neural Networks*, Nov./Dec. 1995, vol. 2, pp. 905–910.

[14] N. Pecharanin, H. Mitsui, and M. Sone, "Harmonic detection by using neural network," in *Proc. IEEE Int. Conf. Neural Networks*, Nov./Dec. 1995, vol. 2, pp. 923–926.

[15] B. Burton and R. G. Harley, "Reducing the computational demands of continually online-trained artificial neural networks for system identification and control of fast processes," *IEEE Trans. Ind. Appl.*, vol. 34, no. 3, pp. 589–596, May/Jun. 1998.

[16] H. Simon, *Neural networks—A comprehensive foundation*, 2nd ed. Englewood Cliffs, NJ: Prentice Hall, 1998.

[17] S. Lee and H. Song, "A new recurrent neural network architecture for visual pattern recognition," *IEEE Trans. Neural Networks*, vol. 8, no. 2, pp. 331–340, Mar. 1997.

[18] E. B. Baum and D. Haussler, "What size net gives valid generalization?," in *Proc. Neural Comput.*, 1989, vol. 1, no. 1, pp. 151–160.

[19] L. Sainz, J. J. Mesas, and S. Herraiz, "" Study of harmonic cancellation between AC/DC converter currents," in *Proc. Int. Conf. Harmon. Qual. Power (ICHQP'04)*, Sep. 2004, pp. 148–153.

[20] P. Cheng, S. Bhattacharya, and D. Divan, "Experimental verification of dominant harmonic active filter for high power applications," *IEEE Trans. Ind. Appl.*, vol. 36, no. 2, pp. 567–577, Mar./Apr. 2000.

[21] F. Z. Peng, "Application issues of active power filters," *IEEE Ind. Appl. Mag.*, vol. 4, no. 5, pp. 21–30, Sep./Oct. 1998.

[22] L. Qian, D. Cartes, L. Hui, and S. K. Srivastava, "A reconfigurable induction motor drive with harmonic cancellation feature," in *Proc. IEEE Elect. Ship Technol. Symp.*, Jul. 2005, pp. 93–98.

Ronald G. Harley (M'77–SM'86–F'92) received the M.Sc.Eng. degree (with honors) in electrical engineering from the University of Pretoria, Pretoria, South Africa, in 1965 and the Ph.D. degree from London University, London, U.K., in 1969.

In 1971, he was appointed to the Chair of Electrical Machines and Power Systems at the University of Natal, Durban, South Africa, and later he became the Department Head and Deputy Dean of Engineering. He is currently the Duke Power Company Distinguished Professor at the Georgia Institute of Technology, Atlanta. He has co-authored some 400 papers and three patents. Altogether, ten of the papers attracted prizes from journals and conferences. His research interests include the dynamic behavior and condition monitoring of electric machines, motor drives, power systems and their components, and controlling them by the use of power electronics and intelligent control algorithms.

Dr. Harley received the Cyrill Veinott Award in 2005 from the IEEE Power Engineering Society for Outstanding contributions to the field of electromechanical energy conversion. He is a Fellow of the British IEE and the Royal Society in South Africa, and a Founder Member of the Academy of Science in South Africa formed in 1994. During 2000 and 2001, he was one of the IEEE Industry Applications Society's six Distinguished Lecturers. He was the Vice-President of Operations of the IEEE Power Electronics Society (2003–2004) and Chair of the Atlanta Chapter of the IEEE Power Engineering Society. He is currently the Publications Chair for IEEE Power Electronics Society, and Chair of the Distinguished Lecturers and Regional Speakers program of the IEEE Industry Applications Society.

Frank C. Lambert (SM'90) received the B.E.E. and M.S.E.E. degrees in electric power engineering from the George Institute of Technology (Georgia Tech), Atlanta, in 1973 and 1976, respectively.

He is the Electrical Systems Program Manager at NEETRAC, Georgia Tech. He worked for the Georgia Power Company from 1973 to 1995, gaining experience in distribution and transmission engineering, operations, and management. He joined NEETRAC in 1996 to manage the Electrical Systems Research Program and is active in PES, where he serves on several working groups in the Distribution Subcommittee.

Ganesh K. Venayagamoorthy (A'91–M'97 –SM'02) received the B.Eng. degree (with first-class honors) in electrical and electronics engineering from the Abubakar Tafawa Balewa University, Bauchi, Nigeria, in 1994 and the M.Sc. and Ph.D. degrees in electrical engineering from the University of Natal, Durban, South Africa, in 1999 and 2002, respectively.

He was a Senior Lecturer at Durban Institute of Technology prior to joining the University of Missouri-Rolla as an Assistant Professor in the Department of Electrical and Computer Engineering in May 2002. His research interests are in computational intelligence, power systems stability and control, evolvable hardware, and signal processing. He has published over 200 papers in refereed journals and international conferences.

Dr. Venayagamoorthy received the 2005 IEEE Industry Application Society (IAS) Young Outstanding Member award, the 2005 South African Institute of Electrical Engineers Young Achievers award, a University of Missouri-Rolla Faculty Excellence award, a 2004 National Science Foundation CAREER award, the 2004 IEEE St. Louis Section Outstanding Young Engineer award, the 2003 International Neural Network Society (INNS) Young Investigator award, and was the recipient of five prize papers with the IEEE Industry Applications Society and IEEE Computational Intelligence Society. He is listed in the 2007 edition of *Who's Who in America*. He is an Associate Editor of the IEEE TRANSACTIONS ON NEURAL NETWORKS, a Senior Member of the South African Institute of Electrical Engineers, and a Member of INNS and the American Society of Engineering Education. He is currently the Chair of the Task Force on Intelligent Control Systems of IEEE Power Engineering Society. He is also the IEEE St. Louis CIS and IAS Chapter Chairs and the Chair of the IEEE CIS Task Force on Power System Applications.

Joy Mazumdar (S'00–M'06) received the B.S. degree in electronics engineering from Shivaji University, Kolhapur, India, in 1994, the M.S degree in electrical engineering from the University of Central Florida, Orlando, in 2002, and the Ph.D. degree in electrical engineering from the Georgia Institute of Technology, Atlanta, in 2006.

He is currently with the Power Conversion Division, Siemens Energy and Automation, Alpharetta, GA, as a Senior Systems Engineer. Prior to joining graduate school, he was with Siemens, Ltd., India, from 1995 to 2000 as a Power Electronics Engineer. His current responsibilities include design and new application development for active front ends, power system studies leading to utility compliance, and utility scale energy storage. His other research focuses on the development of power systems harmonics monitoring tool using neural network techniques. He is the joint holder of two patents, one issued and one pending. His research interests include utility applications of power electronics, power quality issues, active filters, inverter design for renewable energy systems, switching power supplies, variable speed drives, and control techniques.